Rare Met. (2022) 41(9):3160–3169
https://doi.org/10.1007/s12598-022-02040-y

RARE METALS

ORIGINAL ARTICLE

Skyrmion-(non)crystal structure stabilized by dipolar interaction

Ming-Xiu Sui, Yong Hu*

Received: 1 November 2021 / Revised: 22 January 2022 / Accepted: 29 January 2022 / Published online: 2 July 2022

Abstract We report a numerical study on the role of long-range dipolar interaction played on the creation and stabilization of skyrmion-(non)crystal structure in chiral ferromagnetic thin films without any anisotropies, based on a Monte-Carlo simulation method. With the increase of external magnetic field, the microscopic spin configuration is transformed from a spin-spiral stripe or labyrinth structure, depending on the strength of dipolar interaction, into a skyrmion-(non)crystal structure, and then into a skyrmion-gas structure, and finally into a ferromagnetic state. Interestingly, with the increase of dipolar interaction, the skyrmion-crystal structure evolves from a triangular arrangement into a square arrangement with the change of skyrmion shape from circle to square. For larger dipolar interactions, the skyrmion-crystal structure loses the regular arrangements and the skyrmions, remaining topological, exhibit different shapes and sizes and squeeze with each other, whose distributions are analogous to a non-crystal structure. Therefore, different skyrmion-(non)crystal structures are stabilized in different ranges of dipolar interactions, which further promotes the applications of skyrmions as non-volatile information carriers.

Keywords Chiral ferromagnetic thin film; Skyrmion-(non)crystal structure; Interfacial Dzyaloshinskii-Moriya interaction; Dipolar interaction; Monte-Carlo simulation

M.-X. Sui, Y. Hu*
Department of Physics, College of Sciences, Northeastern University, Shenyang 110819, China
e-mail: huyong@mail.neu.edu.cn

Y. Hu
State Key Laboratory of Rolling and Automation, Northeastern University, Shenyang 110819, China

1 Introduction

Recently, the creation and manipulation of magnetic skyrmions, as a promising approach to realize the next-generation, ultra-low power memory and logic devices [1–4], have become one of the hottest topics of contemporary physics. Skyrmions can be employed as non-volatile information carriers in magnetic media, i.e., the presence of a skyrmion can stand for a binary information digit '1' or '0'. Hence, the controllable and reliable creation and annihilation of skyrmions are prerequisites for any skyrmion-based information storage applications. The efficiency of a skyrmion-based nanodevice relies on magnetic skyrmions' nontrivial topology, and a magnetic skyrmion generally exists as a vortex-like swirling spin texture with a nonzero integer skyrmion number (q) defined by:

$$q = \frac{1}{4\pi}\int \hat{\boldsymbol{n}} \cdot \left(\frac{\partial \hat{\boldsymbol{n}}}{\partial x} \times \frac{\partial \hat{\boldsymbol{n}}}{\partial y}\right) \mathrm{d}x\mathrm{d}y \tag{1}$$

which represents how many times the spin directions wrap a unit sphere [5, 6]. Here, the integral is taken over the two-dimensional (2D) magnetic unit cell, and $\hat{\boldsymbol{n}} = \boldsymbol{m}(\mathbf{r})/|\boldsymbol{m}(\mathbf{r})|$ is the unit vector that points along the local magnetic moment ($\boldsymbol{m}(\mathbf{r})$). This indicates that a magnetic skyrmion has the character of a countable particle, and for an individual skyrmion, the integral over its size usually yields $q = \pm 1$; while for skyrmion-crystal structures, the natural measure is the density of topological charge, whose quantity is of prime importance as the topological contribution proportional to the Hall resistivity [7, 8].

Magnetic skyrmions were first introduced theoretically and discovered experimentally in magnetic materials with broken inversion symmetry [9, 10], where magnetic interactions imposed by the chirality of underlying

crystallographic structure, known as Dzyaloshinskii-Moriya interactions (DMI) [11], provide a physical mechanism that prevents the collapse and stabilizes the axisymmetric localized states with finite sizes. DMI naturally presents in a variety of bulk chiral magnets [10, 12–15], while at the interface between an ultrathin magnetic film and a nonmagnetic film with a large spin–orbit coupling (SOC), the DMI can also be induced with the energy given as [16]:

$$E_{\mathrm{DMI}} = d\sum_{\langle ij\rangle}\left(\hat{\boldsymbol{r}}_{ij}\times\hat{\boldsymbol{z}}\right)\cdot\left(\hat{\boldsymbol{m}}_i\times\hat{\boldsymbol{m}}_j\right) \tag{2}$$

where d is the interface-induced DMI energy, $\hat{\boldsymbol{r}}_{ij}$ is the unit vector between spin i and j, $\hat{\boldsymbol{m}}_i$ and $\hat{\boldsymbol{m}}_j$ are the reduced magnetic spin vectors, and $\hat{\boldsymbol{z}}$ is the normal to the interface determined by Moriya's rule [17], oriented from the large SOC material to the magnetic film. The interfacial DMI allows stabilizing the so-called Néel skyrmions [18], also known as hedgehog-like configurations, which are characterized by a nonzero contribution in the radial direction. Comparative advantages of the Néel skyrmions in thin films over the Bloch skyrmions, commonly stabilized in bulk chiral magnets, involve that the nanoscale ultrathin-film structures are preferred for the ultrahigh-density magnetic recording [19] and the Néel skyrmions have been stabilized even at room temperature [2, 20, 21].

For the skyrmion-crystal structures, a close-packed triangular arrangement of skyrmions is usually favored irrespective of the underlying crystal symmetry [10, 12–15]. However, a square skyrmion-crystal structure was also observed probably due to the roles of additional energy terms, such as four-spin interactions [18, 22], dipolar interactions [23] and anisotropies [24, 25]. Theoretical calculations have predicted that the strong enough in-plane anisotropies encourage the skyrmion growth, resulting in the change of skyrmion-crystal structure from triangular to square and further the overlaps of adjacent skyrmions. The skyrmions become expanded and deformed due to their squeezing, and the skyrmions with different sizes coexist to form a noncrystal-like structure [25–27]. On the other hand, the dipolar interactions are commonly small and thus neglected in ultrathin films due to the zero-thickness limit [28], while with the increase of layer thickness, the dipolar interactions in ferromagnets are strengthened normal to the film plane and usually impede to the formation of ultrasmall skyrmions [29]. In other words, the magnetic dipolar interaction was considered to lead to large micrometer-sized magnetic bubbles [30], and its role played on the skyrmion formation in the presence of tunable DMI and/or magnetocrystalline anisotropies has been studied recently, such as the stabilization of specific skyrmion-crystal structures [23, 24], the formation of Néel caps which entail a change from clockwise chirality at the top of the film to counterclockwise chirality at the bottom [31], and the coexistence of Néel- and Bloch-typed skyrmions [32]. It has been suggested that the dipolar forces can provide momentum-dependent biaxial anisotropies in the reciprocal space, which leads to the double-Q modulated spin structure (square skyrmion-crystal structure) stabilization based on the spin-wave theory [23]. In this work, the role of dipolar interaction played on the creation and annihilation of skyrmions in a chiral ferromagnetic thin-film under an external magnetic field is studied numerically, and it is found that the triangular and square skyrmion-crystal and disordered skyrmion-noncrystal structures are induced in different ranges of dipolar interactions in the absence of anisotropy.

2 Model

A coarse-grained ferromagnetic film model is established, where 100 × 100 spins are selected and placed on the node of a 2D square lattice with a lattice constant (a) and periodic boundary conditions being considered. Hence, the skyrmion size is in unit of (a), and the experimental heterostructures and complex crystal structures that are used to generate the interfacial DMI are represented by a variety of energy terms. For a chiral ferromagnetic thin film, the energy can be given as:

$$E = E_{\mathrm{EXC}} + E_{\mathrm{DMI}} + E_{\mathrm{DIP}} + E_{\mathrm{ZEEM}} \tag{3}$$

where

$$E_{\mathrm{EXC}} = -j\sum_{\langle ij\rangle}\hat{\boldsymbol{m}}_i\cdot\hat{\boldsymbol{m}}_j \tag{4}$$

$$E_{\mathrm{DIP}} = -\frac{g}{r_{ij}^3}\sum_{ij}\left[3\left(\hat{\boldsymbol{m}}_i\cdot\hat{\boldsymbol{r}}_{ij}\right)\left(\hat{\boldsymbol{m}}_j\cdot\hat{\boldsymbol{r}}_{ij}\right)-\hat{\boldsymbol{m}}_i\cdot\hat{\boldsymbol{m}}_j\right] \tag{5}$$

$$E_{\mathrm{ZEEM}} = -h\sum_i\hat{\boldsymbol{m}}_i \tag{6}$$

The first term is the ferromagnetic exchange energy (E_{EXC}) with an exchange constant j, which determines the Curie temperature and serves as an energy unit to reduce other parameters to be dimensionless. The second term is the interfacial DMI energy (E_{DMI}, given in Eq. (2)) with a fixed constant $d = 0.7j$, which is larger than those used in analytical ($\sim 0.1j - 0.2j$) and ab initio (up to $0.3j$) calculations [1] and slightly smaller than that ($1.0j$) used in Monte-Carlo simulations by others [24, 33]. Remarkably, the value of d/j depends on the theoretical method and its value determines the wavelength of spin-spirals and the diameter and density of skyrmions [34]. The third term is the long-range dipolar interaction energy (E_{DIP}) with a tunable constant g ranging from 0 to $0.3j$. The long-range dipolar interactions arise from the interactions of electromagnetic field of magnetic dipoles, e.g., protons, electrons, nuclei, and are ubiquitous probably to play

nonnegligible roles in ferromagnetic nanostructures. In addition to the spin separations, the magnetic moment values of coupled spins and the stray fields induced by the sample shape can determine and change the value of dipolar interaction [35, 36]. The last term is the Zeeman energy (E_{ZEEM}) with a reduced value $h/j = \mu_0 H M_S/j$, where μ_0 is the permeability of vacuum, H is the magnetic field strength, and M_S is the saturated magnetization, and the h value can also vary from 0 to $1.3j$ to establish the phase diagram.

In the Monte-Carlo simulation, the initial magnetic states are disordered and a field-annealed process is conducted from $T = 1.0j/k_B$ to $0.01j/k_B$ in steps of $0.01j/k_B$ in order to avoid the spins to be trapped in a frustrated state whose energy has not been globally minimized yet at the target temperature. In other words, the field-annealed process in the simulation is necessary to obtain the magnetically topologically protected textures. Furthermore, the target temperature of $T = 0.01j/k_B$ is low enough to stabilize the spin configuration states even for the dense skyrmion-(non)crystal structures. In order to obtain a complete magnetic phase diagram with respect to h and g, the increments of h are $0.03j$ for $g \leq 0.10j$ and $0.05j$ for $g > 0.10j$, respectively, and for precisely determining the h–g sites of the magnetic phase boundaries and the maximum skyrmion densities with h, and the increment of h related to the skyrmion configurations may be $0.01j$. Note that the ranges of h and g used here seem to be greater than those reported experimentally, which commonly occurs in the Monte-Carlo simulation studies on skyrmions [12, 24]. Yu et al. [12] used a Monte-Carlo method with higher magnetic parameter values to simulate the temperature-field phase diagram involving a triangular skyrmion-crystal structure in a thin film of $Fe_{0.5}Co_{0.5}Si$, and the theoretical and experimental results show good agreement not only in the behavior of the phase change between the helical structure and the skyrmion-crystal structure, but also in the transitional coexistence regions of the helical (or ferromagnetic) structure and the skyrmion-crystal structure. On the other hand, Komatsu et al. [24] numerically studied the role of Ising anisotropy on spin configurations and their evolutions at different dipolar interactions (0, $0.3j$ and $0.6j$), and a complete magnetic phase transition from a helical structure to a square skyrmion-crystal structure and finally to a ferromagnetic structure with h was obtained. One possible reason for the inconsistence of parameters such as h and g between simulation and experiment is that the pinning effect due to, for example, imperfections in the crystal is not taken into account in the simulation. Another possibility, which might be more fundamental, is that the real system has a finite thickness and sufficient spins whereas the simulation was carried out for a purely 2D model with a much smaller size [12, 37, 38]. Furthermore, based on the conventional Monte-Carlo method, the use of model size with dipolar interactions should be highly limited due to the long-range character, resulting in an $O(N^2)$ computational time, representing the computational time proportional to the square of the total number of spins (N). Therefore, the stochastic cutoff (SCO) method is adopted to reduce the computational cost down to $O(N)$ [24, 39]. For the update of spin state at each temperature, 10,000 Monte-Carlo steps are performed, involving the first 8000 Monte-Carlo steps to equilibrate the system and be discarded, and the following 2000 Monte-Carlo steps where the physical quantities such as magnetization, energy and spin orientation are averaged.

3 Results and discussion

At first, the results of the normalized magnetization ($m = M/M_S$) with different h and g are shown in Fig. 1a. In order to indicate the m variations with g under low and high h, the results of $m = 0.2$ and 0.8 are labeled. Without g, m increases from 0 to 0.2 with the increase of h from 0 to $0.1j$ and rapidly approaches to and above 0.8 as h is higher than $0.4j$. When g is taken into account and initially increases to $\sim 0.15j$, the m-h behaviors under low h are insensitive to g, i.e., m increases to 0.2 when h is close to $0.1j$. At larger g ($> 0.15j$), m gets 0.2, which needs higher h values with the increase of g. Under high h, the h value of $m = 0.8$ roughly linearly increases with the increase of g, and the slope of h-g line when $g > 0.16j$ is larger than that for smaller g, as shown in Fig. 1a. When m increases with the increase of h at a given g, the microscopic spin configuration evolves to minimize the system energy, and the phase transitions may happen, resulting in the sharp changes in the magnetization. To target these h–g sites precisely, the h partial derivative of m ($\partial m/\partial h$) for a given g is calculated with the selected results presented in Fig. 1b, c.

The results show that, $\partial m/\partial h$ is bimodal with h for small g (Fig. 1b) while unimodal for large g (Fig. 1c). The peaks under low h are insensitive to g before they disappear, while under high h, the peak roughly equidistantly moves to higher h with the increase of g and the peak value decreases. When the peak under low h disappears or appears under zero h with the increase of g, the other peak under high h becomes rounded and sensitive to g, and the $\partial m/\partial h$-h curve becomes abnormal under high h as $g \geq 0.25j$, indicating that too large g may induce unexpected complex magnetization behaviors and beyond the scope of this work. The h and g values corresponding to the peaks of $\partial m/\partial h$ have been extracted and plotted in Fig. 1a by spheres. The consistence between spheres and solid curves of $m = 0.2$ and 0.8 indicates that the phase transition with

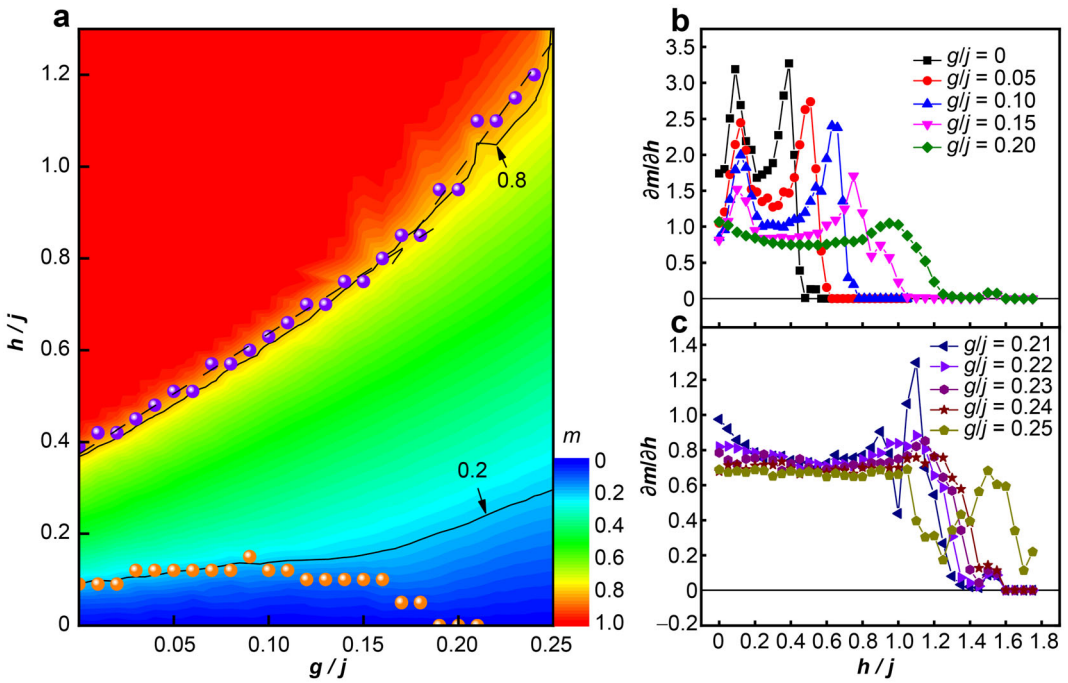

Fig. 1 **a** Normalized magnetization (m) as a function of external magnetic field (h) and dipolar interaction (g); **b**, **c** h partial derivative of m ($\partial m/\partial h$) as a function of h for selected g (spheres in **a** indicating (h, g) coordinates corresponding to peaks of $\partial m/\partial h$ in **b**, **c**; dashed lines in **a** being linearly fit results; curves of m = 0.2 and 0.8 being labeled in **a** for discussing m variations with g and h)

h occurs at these two m values. The simple correspondence implies that the m value could also be as a probe tool to identify the phase boundary for specific g. However, the inconsistence under low h at large g due to the loss of $\partial m/\partial h$ peak shows a distinct character of phase transition.

Next, the microscopic spin configurations for different h and g are calculated and the selected results are depicted in Fig. 2. Without g, a spin-spiral stripe structure with alternate spin-up and spin-down states is formed under zero h due to the energy competition between j and d. Different from some micromagnetic results of ground state where only the parallel stripes are obtained, some turnings emerge probably because thermal fluctuations are allowed in the Monte-Carlo simulation and thus some nucleation sites remain at low temperature. When h is introduced and initially increases ($h = 0.09j$ in Fig. 2a), the long stripes are cut off into point- or bar-typed pieces of the spin-down domains separated by spin-up domains. With the increase of h to an appropriate value ($h = 0.24j$ in Fig. 2a), the microscopic spin configuration evolves into a skyrmion-crystal structure with a triangular arrangement, i.e., each skyrmion is circular and has a coordinate number of six. With the further increase of h, the skyrmion-crystal structure is broken, and the reduced skyrmions distribute randomly in a ferromagnetic domain to form a so-called skyrmion-gas structure. Finally, the skyrmions completely disappear and a fully ferromagnetic domain with spins parallel to h is stabilized under higher h.

When g is introduced and increases ($g = 0.06j$ and $0.12j$ shown in Fig. 2b, c), the long stripes of the ground state under $h = 0$ favor to be formed, even a completely parallel stripe observed for $g = 0.12j$. In Komatsu et al.'s work [24], the dipolar interactions change the helical phase from a diagonal to a vertical direction, meanwhile, expand the helical phase region to the positive anisotropy direction. Nevertheless, in this work, although the Monte-Carlo simulations are performed on a similar crystal-structure model, the directional change of the helical phase alignment from zero to nonzero g is not observed, which is probably due to the lack of anisotropy energy term in Eq. (3). With the increase of h, the stripe structure is still changed into the skyrmion-crystal structure. However, the existence of g in thin film resembles an in-plane shape anisotropy to make spins lie in the film plane [40]. Hence, the skyrmion size is larger with the increase of g, which also agrees with the common knowledge of dipolar-induced skyrmions with a large size [30]. Interestingly, the enlarged skyrmions make their arrangement closer and the ferromagnetic domains around them are compressed. Consequently, the skyrmion shape transforms from circle into square, and the coordinate number may decrease. The high enough h changes the skyrmion-crystal into skyrmion-gas structure, and the skyrmions disappear under a higher h at a larger g.

When g increases to $0.18j$, many spins are favored to be flat in the film plane. At the ground state under zero h, the

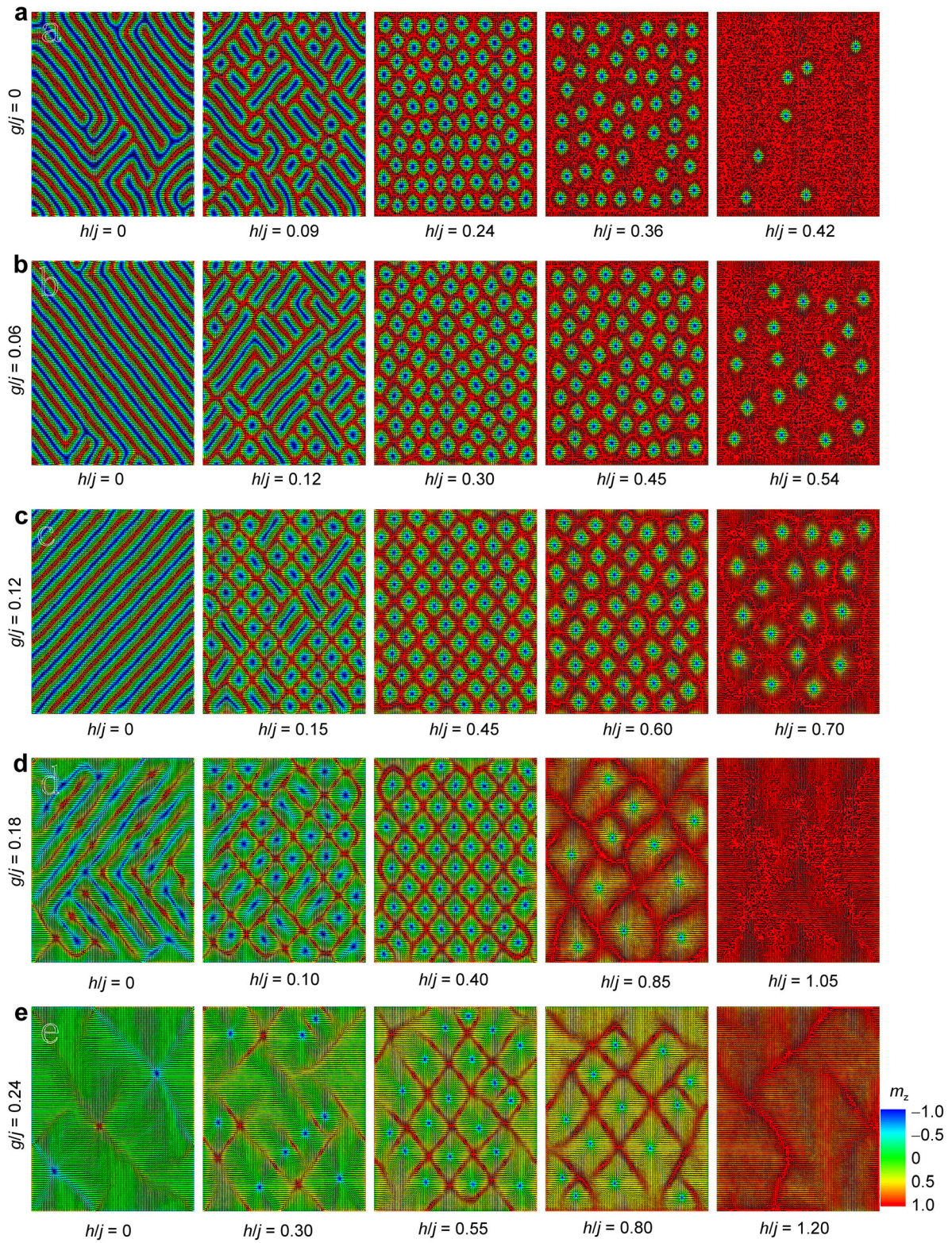

Fig. 2 Spin configurations under different *h* for selected *g*, where colors give *z* component results of magnetization and arrows represent spin orientations

spin-spiral separation between spin-up and spin-down domains is extended while the spin-up and spin-down domain widths are reduced due to the constant periodicity for a fixed *d*/*j*, and the orthogonal stripes with turnings

emerge. With the increase of h, the helical stripe structure evolves into the skyrmion-crystal structure, and significantly, the skyrmions seem to be square-shaped and thus the square lattice of skyrmions, each of which has a coordinate number of four, is stabilized to minimize the system energy. The skyrmion-crystal structure is broken under a higher h, while the skyrmions deform to have different sizes and squeeze with each other before they ultimately vanish under high enough h. For $g = 0.24j$, most spins are stabilized to lie in the film plane and no helical stripe structure is observed at the ground state under zero h due to the too strong dipolar interaction. With the increase of h, the skyrmions with different sizes can be still formed and not arranged in a regular crystal structure, similar to the results found in the presence of a strong in-plane anisotropy [25, 26]. Under higher h, the skyrmions are compressed, melt, deformed, and finally disappear, and a spin-cone state may be observed before the formation of a ferromagnetic domain, as shown in Fig. 2e.

As mentioned above, skyrmions can be quantified by q due to their nontrivial topology. In order to reveal the influence of g on the skyrmion density and plot the h–g phase diagram, the results of q calculated by Eq. (1) with different g and h are summarized in Fig. 3. It is found that for small g (below $0.22j$), the low-h value where q becomes nonzero is insensitive to g, while for large g (above $0.22j$), the low-h value to induce a nonzero q depends on g, i.e., the larger the g is, the higher the h is needed. In the high-h range, the value of h to reduce q down to zero is roughly proportional to g for $g < 0.22j$, and for larger g to $0.30j$, the high-h value where q decreases to zero exhibits a fluctuation around a constant value. In the topological states ($q \neq 0$), with the increase of g to $0.22j$, the maximum q value initially increases and then decreases under proper h while the h range of nonzero q is widened; with the further increase of g, q continues decreasing and the h range of nonzero q becomes narrow due to the increase of low-h value where q becomes nonzero with the increase of g. As compared to the critical h-g values where q becomes nonzero (shown by triangles in Fig. 3a) and where the peak values of $\partial m/\partial h$-h curves appear (shown by spheres in Fig. 1a), the data are consistent when g is smaller than $0.22j$, while not for larger g, indicating distinct phase transition features with h between small and large g.

As shown in Figs. 2, 3b–d, different skyrmion-(non)crystal structures have been identified in different g ranges. In order to characterize different skyrmion-(non)crystal structures, the skyrmion center is firstly located by detecting domains in which $m_z < -0.9$ is fulfilled, and then the distances between skyrmion centers are

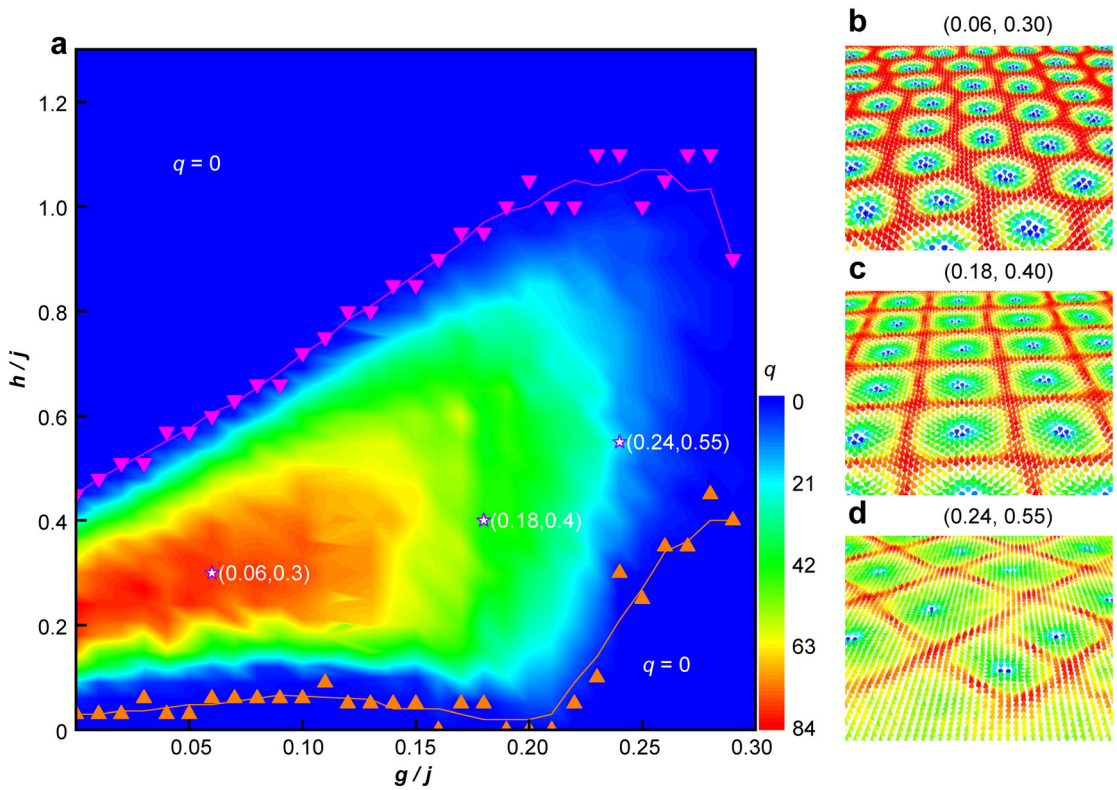

Fig. 3 **a** Skyrmion charge number (q) as a function of h and g, where triangular symbols separate nonzero and zero q zones and curves are guide to eyes; topological spin configurations: **b** triangular skyrmion-crystal structure, **c** square skyrmion-crystal structure and **d** skyrmion-noncrystal structure, whose (g, h) coordinates are labelled

calculated. Apparently, the distance between adjacent skyrmion centers is the smallest, and due to the existence of thermal fluctuations, the smallest distance is defined so long as the distance is smaller than 15a, that is, the coordination number of a skyrmion is counted when the distance from other skyrmion centers to its centers is smaller than 15a. For a skyrmion-(non)crystal structure, the average coordination number of skyrmion (<Z>) and the average smallest distance between skyrmion centers (<L>) are calculated by:

$$Z = \frac{1}{N_{\mathrm{sk}}} \sum_{i=1}^{N_{\mathrm{sk}}} Z_i \tag{7}$$

$$L = \frac{1}{N_{\mathrm{sk}}} \sum_{i=1}^{N_{\mathrm{sk}}} \frac{1}{Z_i} \sum_{nn=1}^{Z_i} L_{i,nn} \tag{8}$$

where Z_i is the coordination number of skyrmion i, $L_{i,nn}$ is the smallest center distance between skyrmion i and the nnth nearest-neighbor skyrmion of skyrmion i, and N_{sk} is the skyrmion number. As shown in Fig. 4a, b, <Z> is close to 6 at g = 0 and decreases monotonically down to nearly 0 with the increase of g from 0 to 0.24j, and the values of <L> fluctuate between 11a and 12a when g is smaller than 0.15j, while fluctuate around 13a for larger g. In the triangular and square skyrmion-crystal structures, the ideal values of <Z> are 6 and 4, respectively, while in the skyrmion non-crystal structure, the skyrmions expand with high size dispersion and the value of <Z> should be equal to or less than 1, which is also evidenced by the results of <L> . The intermediate values of <Z> between 6 and 4 and between 4 and 1 denote the existence of mixed skyrmion-(non)crystal structures. Therefore, the skyrmion-(non)crystal structures can be quantified by <Z> . On the other hand, both <Z> and <L> are insensitive to h, as shown in Fig. 4c, d, and thus the effect of h on the transition between different skyrmion-(non)crystal structures is neglected.

Finally, according to the results of $\partial m/\partial h$ shown in Fig. 1, microscopic spin configuration in Fig. 2, q in Fig. 3, and <Z> and <L> in Fig. 4, the h-g phase diagram is plotted and presented in Fig. 5a. Under zero or a low h, a spin-spiral stripe structure is observed for g smaller than 0.18j, while a labyrinth structure for larger g. With the increase of h, the spin-spiral stripe structure is rapidly transformed into a skyrmion-crystal structure via their mixed phases in a narrow h range at small g. In the skyrmion-crystal structure, the triangular arrangement of circular skyrmions (Fig. 3b) is favored to be stabilized for zero and small g (roughly smaller than g = 0.09j), while

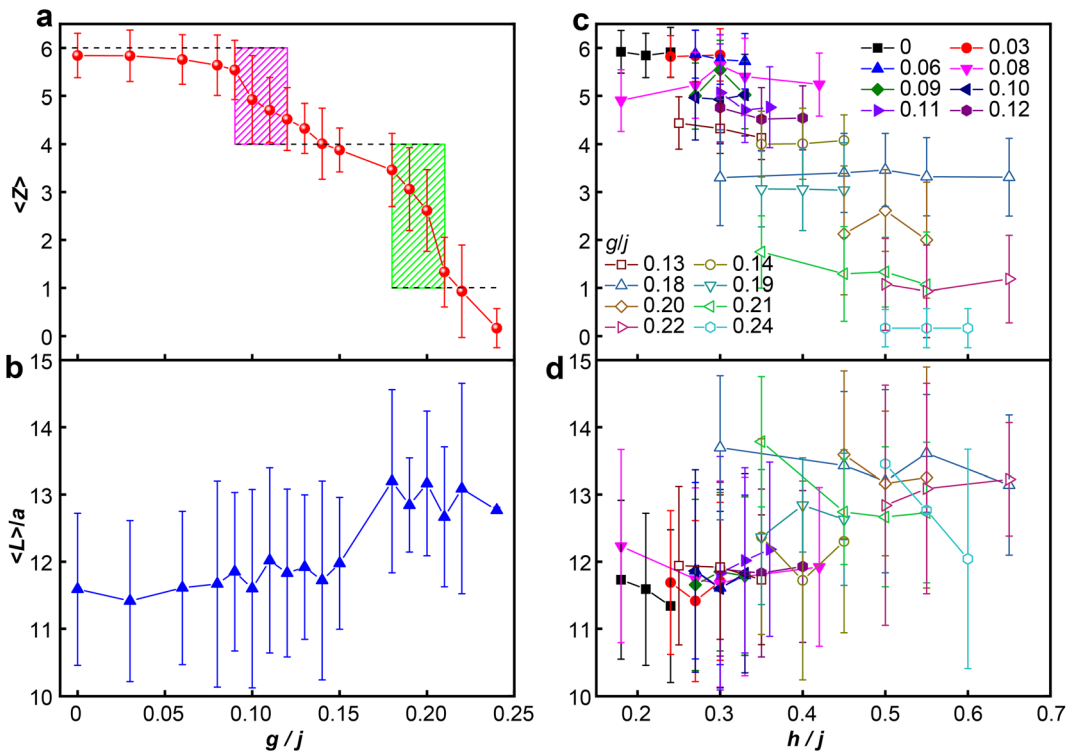

Fig. 4 **a** Average coordination number of skyrmion (<Z>) and **b** average smallest distance between skyrmion centers (<L>/a) as a function of g under external magnetic field h value, where q is maximum, dashed lines point out ideal coordination numbers in triangular (6), square (4) skyrmion-crystal structures and skyrmion-noncrystal structure (1) and shadow areas indicate mixed regions of different skyrmion-(non)crystal structures; **c** <Z> and **d** <L> as a function of h for selected g (error bars being determined by averaging Z of different skyrmions and L between different adjacent skyrmion centers)

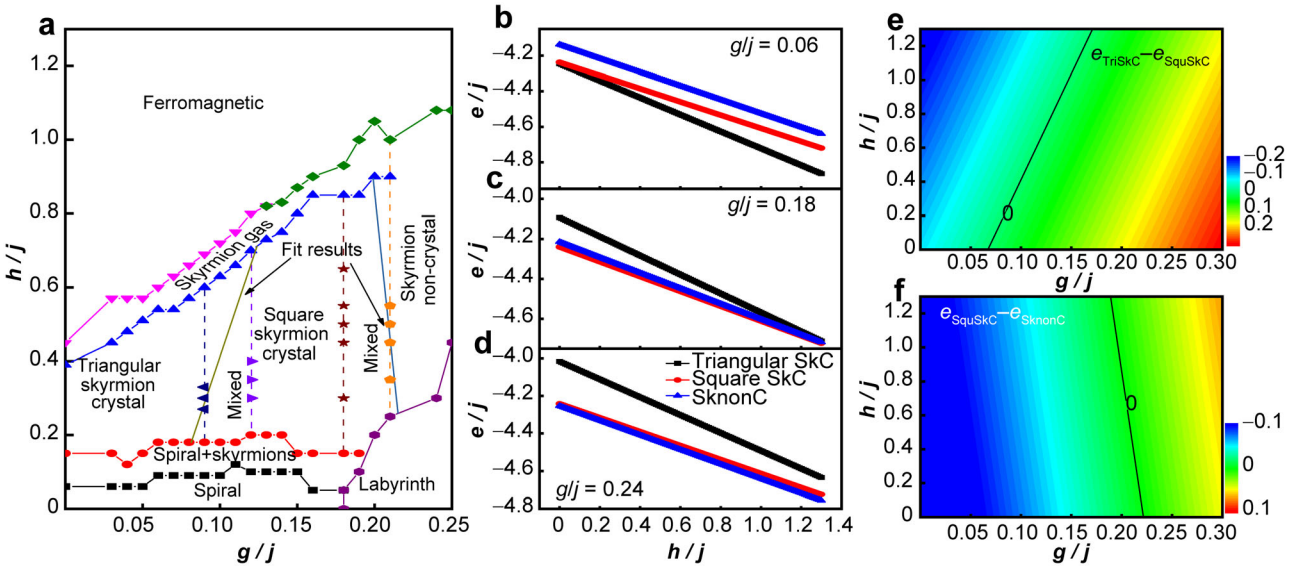

Fig. 5 **a** *h*-*g* phase diagram; energies (*e*) of three skyrmion-(non)crystal structures as a function of *h* for **b** small, **c** intermediate and **d** large *g*; energy difference **e** between triangular skyrmion-crystal (TriSkC) structure and square skyrmion-crystal (SquSkc) structure and **f** between square skyrmion-crystal structure and disordered skyrmion-noncrystal (SknonC) structure as a function of *h* and *g*, where lines of zero energy difference are plotted in **e**, **f** and also labelled in **a**

with the increase of g from $0.09j$ to $\sim 0.18j$, the square arrangement of square skyrmions (Fig. 3c) becomes preferred. For larger g, labyrinth structure exists in a wide low-h range (including under zero h) and with the increase of h, the skyrmions appear with different shapes and sizes, squeeze with each other, and their distribution is analogous to the formation of a noncrystal structure of skyrmions [25, 26]. Under a high h, the skyrmion-crystal structures are broken and transformed into the skyrmion-gas structure due to the annihilation of some skyrmions for small g, and finally, a ferromagnetic spin structure is formed under higher h. For the noncrystal structure of skyrmions at large g, the transition into the ferromagnetic state with the increase of h occurs through an intermediate spin-cone state, which commonly appears in the systems with strong non-collinear couplings under high h [41]. The stabilization of the distinct skyrmion-(non)crystal structures in the individual g range has also been elucidated by comparing their energies, as shown in Fig. 5b–d. The analytic calculations of the energy differences between representative triangular skyrmion-crystal, square skyrmion-crystal and skyrmion-noncrystal structures estimate the *h*-*g* lines of their degenerate states (Fig. 5e, f), which agrees with the results of microscopic spin configurations and $\langle Z \rangle$.

4 Conclusion

In summary, a Monte-Carlo simulation is performed to study the influence of g on the creation and stabilization of skyrmions in chiral ferromagnetic thin films under an external magnetic field. It is found that the skyrmions are triggered and stabilized under proper h, and triangular and square skyrmion-crystal structures and disordered skyrmion-noncrystal structure are successively observed with the increase of g. Commonly, the value of dipolar interaction in bulk materials with specific spins of atoms is constant, while in nanostructures the dipolar interactions may be enhanced when it is able to increase the domain-wall width at the top and bottom of the film with a layer-by-layer basis by modifying the anisotropy, as observed in [Pt/Co/Ir] multilayer systems, because the value of dipolar interaction also depends on the distance and angle between spins and the spin relative motion. Experimentally and theoretically, different typed skyrmion-(non)crystal structures have been found and interpreted based on the contributions of distinct energies. The triangular skyrmion-crystal structure has been directly observed in noncentrosymmetric chiral magnets such as MnSi and $Fe_{0.5}Co_{0.5}Si$ where the DMI and ferromagnetic exchange interactions are competing, or in centrosymmetric achiral frustrated magnets where the second or third antiferromagnetic nearest-neighbor exchange interactions are also taken into account, and the square skyrmion-crystal structure has been reported experimentally in a hexagonal monolayer Fe on Ir(111) and in a centrosymmetric tetragonal magnet $GuRu_2Si_2$, in which the four-spin interactions are significant. Moreover, the triangular and square skyrmion-crystal and disordered skyrmion-noncrystal structures were also observed at different in-plane anisotropies. Therefore, this

work shows a possible scenario of the triangular and square skyrmion-crystal structures and disordered skyrmion-non-crystal structure driven by the DMI with dipolar interactions, in which the four-spin interactions and anisotropies are absent, which not only fertilizes the fundamental understanding of skyrmions, but also confirms that different skyrmion-(non)crystal structures can appear in materials with different dipolar interactions.

Acknowledgements This study was financially supported by the National Natural Science Foundation of China (No. 11774045) and the Joint Research Fund Liaoning-Shenyang National Laboratory for Materials Science (No. 20180510008).

Declarations

Conflict of interests The authors declare that they have no conflict of interest.

References

[1] Fert A, Cros V, Sampaio J. Skyrmions on the track. Nat Nanotech. 2013;8(3):152.
[2] Woo S, Litzius K, Krüger B, Im MY, Caretta L, Richter K, Mann M, Krone A, Reeve RM, Weigand M, Agrawal P, Lemesh I, Mawass MA, Fischer P, Kläui M, Beach GSD. Observation of room-temperature magnetic skyrmions and their current-driven dynamics in ultrathin metallic ferromagnets. Nat Mater. 2016;15(5):501.
[3] Jiang W, Chen G, Liu K, Zang J, te Velthuis SGE, Hoffmann A. Skyrmions in magnetic multilayers. Phys Rep. 2017;704:1.
[4] Zhang X, Zhou Y, Song KM, Park TE, Xia J, Ezawa M, Liu X, Zhao W, Zhao G, Woo S. Skyrmion-electronics: writing, deleting, reading and processing magnetic skyrmions toward spintronic applications. J Phys Condens Matter. 2020;32(14):143001.
[5] Belavin AA, Polyakov AM. Metastable states of two-dimensional isotropic ferromagnets. JETP Lett. 1975;22:245.
[6] Nagaosa N, Tokura Y. Topological properties and dynamics of magnetic skyrmions. Nat Nanotech. 2013;8(12):899.
[7] Neubauer A, Pfleiderer C, Binz B, Rosch A, Ritz R, Niklowitz PG, Böni P. Topological hall effect in the a phase of MnSi. Phys Rev Lett. 2009;102(18):186602.
[8] Qin PX, Yan H, Wang XN, Feng ZX, Guo HX, Zhou XR, Wu HJ, Zhang X, Leng ZGG, Chen HY, Liu ZQ. Noncollinear spintronics and electric-field control: a review. Rare Met. 2020;39(2):95.
[9] Bogdanov AN, Yablonskii DA. Thermodynamically stable 'vortices' in magnetically ordered crystals. The mixed state of magnets. Sov Phys JETP. 1989;68:101.
[10] Mühlbauer S, Binz B, Jonietz F, Pfleiderer C, Rosch A, Neubauer A, Georgii R, Böni P. Skyrmion lattice in a chiral magnet. Science. 2009;323(5916):915.
[11] Dzyaloshinskii IE. Theory of helicoidal structures in antiferromagnets. Sov Phys JETP. 1964;19:960.
[12] Yu XZ, Onose Y, Kanazawa N, Park JH, Han JH, Matsui Y, Nagaosa N, Tokura Y. Real-space observation of a two-dimensional skyrmion crystal. Nature (London). 2010;465(7300):901.
[13] Wei WS, He ZD, Qu Z, Du HF. Dzyaloshinsky-Moriya interaction (DMI)-induced magnetic skyrmion materials. Rare Met. 2021;40(11):3076.
[14] Kézsmárki I, Bordács S, Milde P, Neuber E, Eng LM, White JS, Rønnow HM, Dewhurst CD, Mochizuki M, Yanai K, Nakamura H, Ehlers D, Tsurkan V, Loidl A. Néel-type skyrmion lattice with confined orientation in the polar magnetic semiconductor GaV_4S_8. Nature Mater. 2015;14(11):1116.
[15] Seki S, Yu XZ, Ishiwata S, Tokura Y. Observation of skyrmions in a multiferroic material. Science. 2012;336(6078):198.
[16] Wiesendanger R. Nanoscale magnetic skyrmions in metallic films and multilayers: a new twist for spintronics. Nat Rev Mater. 2016;1(7):16044.
[17] Moriya T. Anisotropic superexchange interaction and weak ferromagnetism. Phys Rev. 1960;120(1):91.
[18] Heinze S, Bergmann KVON, Menzel M, Brede J, Kubetzka A, Wiesendanger R, Bihlmayer G, Blügel S. Spontaneous atomic-scale magnetic skyrmion lattice in two dimensions. Nat Phys. 2011;7(9):713.
[19] Bader SD. Colloquium: opportunities in nanomagnetism. Rev Mod Phys. 2006;78(1):1.
[20] Boulle O, Vogel J, Yang H, Pizzini S, Souza Chaves DDE, Locatelli A, Menteş TO, Sala A, Buda-Prejbeanu LD, Klein O, Belmeguenai M, Roussigné Y, Stashkevich A, Chérif SM, Aballe L, Foerster M, Chshiev M, Auffret S, Miron IM, Gaudin G. Room-temperature chiral magnetic skyrmions in ultrathin magnetic nanostructures. Nat Nanotech. 2016;11(5):449.
[21] Moreau-Luchaire C, Moutafis C, Reyren N, Sampaio J, Vaz CAF, Horne NVAN, Bouzehouane K, Garcia K, Deranlot C, Warnicke P, Wohlhüter P, George JM, Weigand M, Raabe J, Cros V, Fert A. Additive interfacial chiral interaction in multilayers for stabilization of small individual skyrmions at room temperature. Nat Nanotech. 2016;11(5):444.
[22] Khanh ND, Nakajima T, Yu X, Gao S, Shibata K, Hirschberger M, Yamasaki Y, Sagayama H, Nakao H, Peng L, Nakajima K, Takagi R, Arima T, Tokura Y, Seki S. Nanometric square skyrmion lattice in a centrosymmetric tetragonal magnet. Nat Nanotechnol. 2020;15(6):444.
[23] Utesov OI. Thermodynamically stable skyrmion lattice in a tetragonal frustrated antiferromagnet with dipolar interaction. Phys Rev B. 2021;103(6):064414.
[24] Komatsu H, Nonomura Y, Nishino M. Phase diagram of the two-dimensional dipolar Heisenberg model with Dzyaloshinskii-Moriya interaction and Ising anisotropy. Phys Rev B. 2021;103(21):214404.
[25] Lin SZ, Saxena A, Batista CD. Skyrmion fractionalization and merons in chiral magnets with easy-plane anisotropy. Phys Rev B. 2015;91(22):224407.
[26] Sui MX, Zhang ZB, Chi XD, Zhang JY, Hu Y. Dense skyrmion crystal stabilized through interfacial exchange coupling: role of in-plane anisotropy. Front Phys. 2021;16(2):23501.
[27] Zhang ZB, Hu Y. Zero-field skyrmions in FeGe thin films stabilized through attaching a perpendicularly magnetized single-domain Ni layer. Chin Phys B. 2021;30(7):077503.
[28] Rohart S, Thiaville A. Skyrmion confinement in ultrathin film nanosturctures in the presence Dzyaloshinskii-Moriya interaction. Phys Rev B. 2013;88(18):184422.
[29] Büttner F, Lemesh I, Beach GSD. Theory of isolated magnetic skyrmions: from fundamentals to room temperature applications. Sci Rep. 2018;8(1):4464.
[30] Bogdanov AN, Panagopoulos C. Physical foundations and basic properties of magnetic skyrmions. Nat Rev Phys. 2020;2(9):249.
[31] Lucassen J, Meijer MJ, Jong MCHDE, Duine RA, Swagten HJM, Koopmans B, Lavrijsen R. Stabilizing chiral spin structures via an alternating Dzyaloshinskii-Moriya interaction. Phys Rev B. 2020;102(1):014451.
[32] Bernand-Mantel A, Muratov CB, Simon TM. Unraveling the role of dipolar versus Dzyaloshinskii-Moriya interactions in

stabilizing compact magnetic skyrmions. Phys Rev B. 2020; 101(4):045416.
[33] Nishikawa Y, Hukushima K, Krauth W. Solid-liquid transition of skyrmions in a two-dimensional chiral magnet. Phys Rev B. 2019;99(6):064435.
[34] Simon E, Palotás K, Rózsa L, Udvardi L, Szunyogh L. Formation of magnetic skyrmions with tunable properties in PdFe bilayer deposited on Ir(111). Phys Rev B. 2014;90(9):094410.
[35] Ummelen FC, Lichtenberg T, Swagten HJM, Koopmans B. Controlling skyrmion bubble confinement by dipolar interactions. Appl Phys Lett. 2019;115(10):102402.
[36] Lu Q, Hu Y. Temperature dependence of dipole-induced exchange bias. Nanotechnology. 2020;31(30):305703.
[37] d'Albuquerque e Castro J, Altbir D, Retamal JC, Vargas P. Scaling approach to the magnetic phase diagram of nanosized systems. Phys Rev Lett. 2002;88(23):237202.
[38] Vargas P, Altbir D, d'Albuquerque e Castro J. Fast Monte Carlo method for magnetic nanoparticles. Phys. Rev. B, 2006; 73 (9): 092417
[39] Sasaki M, Matsubara F. Stochastic cutoff method for long-range interacting systems. J Phys Soc Jpn. 2008;77(2):024004.
[40] Yu H, Xiao J, Schultheiss H. Magnetic texture based magnonics. Phys Rep. 2021;905:1.
[41] Hu Y, Chi XD, Li X, Liu Y, Du A. Creation and annihilation of skyrmions in the frustrated magnets with competing exchange interactions. Sci Rep. 2017;7(1):16079.